Characterization of the Strongly Coupled, Low-Frequency Vibrational Modes of the Special Pair of Photosynthetic Reaction Centers via Isotopic Labeling of the Cofactors

Kazimierz Czarnecki,[†] James R. Diers,[†] Veeradej Chynwat,[‡] Joy P. Erickson,[‡] Harry A. Frank,[‡] and David F. Bocian*[,†]

Contribution from the Department of Chemistry, University of California, Riverside, California 92521, and Department of Chemistry, University of Connecticut, Storrs, Connecticut 06269

Received September 18, 1996[⊗]

Abstract: Low-frequency (50−425-cm^{-1}), near-infrared-excitation resonance Raman (RR) spectra are reported for bacterial photosynthetic reaction centers (RCs) from *Rhodobacter sphaeroides* in which the bacteriochlorophyll (BChl) and bacteriopheophytin (BPh) cofactors are labeled with ^{15}N or ^{26}Mg. The focus of the study is the identification of the very low-frequency modes of the dimer of BChls (P) which are strongly coupled to the P* electronic transition which initiates the primary charge separation process in RCs. In order to gain a complete picture of the vibrational characteristics, the low-frequency RR spectra of the accessory BChls and the BPhs were examined in addition to those of P. The RR spectra of the isotopically labeled cofactors in the RCs were compared with one another and with the spectra obtained for solid-film samples of isolated, isotopically labeled BChl and BPh. Based on these comparisons and the predictions of semiempirical normal coordinate calculations, a self-consistent set of assignments has been developed for all the RR active modes of the different BChl and BPh cofactors in the RC which are observed in the very low-frequency regime (50−250 cm^{-1}). The assignments indicate that the strongly coupled, low-frequency modes of P all involve either deformations localized on pyrrole ring I or the macrocycle core. The so-called "marker mode" of P, observed near 135 cm^{-1}, is due to a cluster of three modes, specifically, the in-plane deformation of the C_2-acetyl group (130 cm^{-1}), the doming motion of the Mg(II) ion (137 cm^{-1}), and a core deformation that involves all four pyrrole rings (143 cm^{-1}). The calculations further suggest that the very strongly coupled mode observed near 35 cm^{-1} is due to the out-of-plane deformation of the C_2-acetyl group. The strong coupling of these modes is consistent with the structure of the dimer in which overlap occurs primarily in the region of ring I. This geometrical arrangement of the cofactors also places the C_2-acetyl substituents of one constituent of P in close proximity to the core of the macrocycle of the other. The unique interplay between the structural, electronic, and vibronic characteristics of the primary electron donor suggests that the strong coupling of certain vibrations is an intrinsic consequence of the structure of the dimer and may have important functional ramifications.

Introduction

The reaction center (RC) is a membrane-bound protein responsible for the primary electron-transfer events of photosynthesis.[1−7] Bacterial RCs consist of four bacteriochlorophylls (BChls), two bacteriopheophytins (BPhs), two quinones, a non-heme iron center, a carotenoid, and ∼850 amino acid residues in three polypeptide subunits designated by L, M, and H. The primary electron donor in RCs is a dimer of BChls, designated the special pair or P. The first well-characterized electron-transfer intermediate is the BPh cofactor in the L subunit.[1,3−7] The X-ray crystal structures of RCs from two different purple bacteria (*Rhodobacter sphaeroides* and *Rhodopseudomonas viridis*) have been determined and indicate that P, the accessory BChls, and the BPhs are arranged in the L and M subunits such that the macroscopic symmetry is approximately C_2.[8−10] The arrangement of the BChl and BPh cofactors in RCs from *Rb. sphaeroides* is shown in Figure 1. The structure of BChl *a* (the pigment found in *Rb. sphaeroides*) is shown in Figure 2. In BPh *a*, the Mg(II) ion is replaced by two protons. The Mg(II) ions of the two BChls in P and the two accessory BChls are each ligated to a histidine residue of the protein.[8d,e] This ligation conserves the approximate C_2 symmetry in the RC. This symmetry is broken, however, by inequivalences at other positions of the primary amino acid sequence of the L versus M subunits.

[†] University of California.

[‡] University of Connecticut.

[⊗] Abstract published in *Advance ACS Abstracts,* January 1, 1997.

(1) Kirmaier, C.; Holten, D. *Photosynth. Res.* **1987**, *113*, 225−260.

(2) Deisenhofer, J.; Michel, H. *Science* **1989**, *245*, 1463−1473.

(3) Feher, G.; Allen, J. P.; Okamura, M. Y.; Rees, D. C. *Nature* **1989**, *339*, 111−116.

(4) Boxer, S. G.; Goldstein, R. A.; Lockhart, D. J.; Middendorf, R. T.; Takiff, L. *J. Phys. Chem.* **1989**, *93*, 8280−8294.

(5) Friesner, R. A.; Won, Y. *Biochim. Biophys. Acta* **1989**, *977*, 99−122.

(6) Breton, J., Verméglio, A., Eds. *NATO Ser. A* **1992**, *237*.

(7) Deisenhofer, J., Norris, J. R., Eds. *The Photosynthetic Reaction Center*; Academic: San Diego, CA, 1993; Vol. II.

(8) (a) Deisenhofer, J.; Epp, O.; Miki, R.; Huber, R.; Michel, H. *Nature* **1985**, *339*, 618−624. (b) Deisenhofer, J.; Michel, H. *EMBO J.* **1989**, *8*, 2149−2169. (c) Deisenhofer, J.; Michel, H. *Annu. Rev. Biophys. Biophys. Chem.* **1991**, *20*, 247−266. (d) Ermler, U.; Fritzsch, G.; Buchanan, S.; Michel, H. *Structure* **1994**, *2*, 925−936. (e) Deisenhofer, J.; Epp, O.; Sinning, I.; Michel, H. *J. Mol. Biol.* **1995**, *246*, 429−457.

(9) (a) Allen, J. P.; Feher, G.; Yeates, T. O.; Rees, D. C.; Deisenhofer, J.; Michel, H.; Huber, R. *Proc. Natl. Acad. Sci. U.S.A.* **1986**, *83*, 8589−8593. (b) Allen, J. P.; Feher, G.; Yeates, T. O.; Komiya, H.; Rees, D. C. *Proc. Natl. Acad. Sci. U.S.A.* **1988**, *85*, 8487−8491. (c) Yeates, T. O.; Komiya, H.; Chirino, A.; Rees, D. C.; Allen, J. P.; Feher, G. *Proc. Natl. Acad. Sci. U.S.A.* **1988**, *85*, 7993−7997.

(10) (a) Chang, C.-H.; Tiede, D.; Tang, J.; Smith, U.; Norris, J.; Schiffer, M. *FEBS Lett.* **1986**, *205*, 82−86. (b) Chang, C.-H.; El-Kabbani, O.; Tiede, D.; Norris, J.; Schiffer, M. *Biochemistry* **1991**, *30*, 5352−5360. (c) El-Kabbani, O.; Chang, C.-H.; Tiede, D.; Norris, J.; Schiffer, M. *Biochemistry* **1991**, *30*, 5361−5369.

S0002-7863(96)03281-7 CCC: $14.00

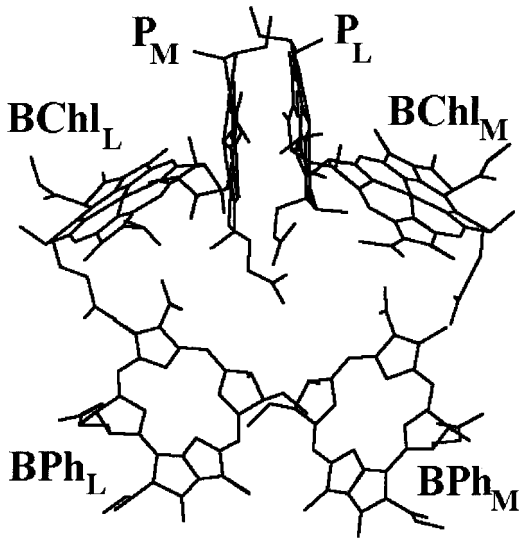

Figure 1. Arrangement of the BChl and BPh cofactors in RCs from *Rb. sphaeroides*. For clarity, the protein matrix, the other cofactors, and the phytyl substituents of the BChls and BPhs have been removed.[8d]

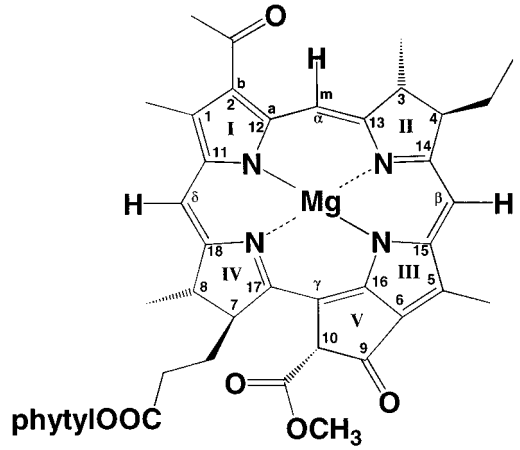

Figure 2. Structure and labeling scheme for BChl *a*.

The X-ray crystallographic data obtained for RCs provide information regarding the distance between and the relative orientation of the cofactors in the protein matrix and serve as benchmarks for the interpretation of spectroscopic data.[8−10] Nevertheless, the practical resolution limits of X-ray crystal structures of large proteins, such as RCs, preclude the elucidation of certain structural features which could be important for determining the functional characteristics of the protein. Vibrational spectroscopy has proven to be an excellent technique for probing the detailed structural properties of the cofactors in RCs. Both resonance Raman (RR), preresonance FT-Raman, and FT-IR techniques have been used to examine wild-type and a number of genetically modified RCs.[11−22] The majority of these vibrational studies have focused on the high-frequency (1000−1750-cm^{-1}) region of the spectrum which contains bands due to the carbonyl and ring-skeletal vibrations of the BChl, BPh, and quinone cofactors.[11−13a,b,e,f,15−22] The vibrational data have been used to assess the conformation of the BChl and BPh rings, the ligation state of the Mg(II) of the BChls, and the extent of hydrogen bonding between the protein residues and the peripheral carbonyl substituents of the various cofactors.

Although most vibrational studies of RCs have focused on the high-frequency modes of the cofactors, the low-frequency vibrational features, particularly those of P, are of considerable interest. Hole-burning[23−25] and second-derivative optical studies[26] on P have shown that very low-frequency modes (30−150 cm^{-1}) are strongly coupled to the P* electronic transition

(11) For reviews, see: (a) Lutz, M. *Adv. Infrared Raman Spectrosc.* **1984**, *11*, 211−300. (b) Lutz, M.; Robert, B. In *Biological Applications of Raman Spectroscopy*; Spiro, T. G., Ed.; Wiley: New York, 1988; Vol. 3, pp 347−411. (c) Lutz, M.; Mäntele, W. In *Chlorophylls*; Scheer, H., Ed.; CRC Press: Boca Raton, FL, 1991; pp 855−902. (d) Lutz, M. *Biospectroscopy* **1995**, *1*, 313−327.

(12) (a) Robert, B.; Lutz, M. *Biochemistry* **1988**, *27*, 5108−5114. (b) Mattioli, T. A.; Hoffman, A.; Robert, B.; Schrader, B.; Lutz, M. *Biochemistry* **1991**, *30*, 4648−4654. (c) Mattioli, T. A.; Robert, B.; Lutz, M. In ref 6, pp 127−132. (d) Mattioli, T. A.; Hoffman, A.; Sockalingum, D. G.; Robert, B.; Lutz, M. *Spectrochim. Acta* **1993**, *49A*, 785−799. (e) Feiler, U.; Albouy, D.; Mattioli, T. A.; Lutz, M.; Robert, B. *Biochemistry* **1994**, *33*, 7594−7599. (f) Mattioli, T. A. *J. Mol. Struct.* **1995**, *347*, 459−466.

(13) (a) Bocian, D. F.; Boldt, N. J.; Chadwick, B. A.; Frank, H. A. *FEBS Lett.* **1987**, *214*, 92−96. (b) Peloquin, J. M.; Violette, C. A.; Frank, H. A.; Bocian, D. F. *Biochemistry* **1990**, *29*, 4892−4898. (c) Donohoe, R. J.; Dyer, R. B.; Swanson, B. I.; Violette, C. A.; Frank, H. A.; Bocian, D. F. *J. Am. Chem. Soc.* **1990**, *112*, 6716−6718. (d) Palaniappan, V.; Aldema, M. A.; Frank, H. A.; Bocian, D. F. *Biochemistry* **1992**, *31*, 11050−11058. (e) Palaniappan, V.; Bocian, D. F. In ref 6, pp 119−126. (f) Palaniappan, V.; Martin, P. C.; Chynwat, V.; Frank, H. A.; Bocian, D. F. *J. Am. Chem. Soc.* **1993**, *115*, 12035−12049.

(14) (a) Shreve, A. P.; Cherepy, N. J.; Franzen, S.; Boxer, S. G.; Mathies, R. A. *Proc. Natl. Acad. Sci. U.S.A.* **1991**, *88*, 11207−11211. (b) Cherepy, N. J.; Shreve, A. P.; Moore, L. J.; Franzen, S.; Boxer, S. G.; Mathies, R. A. *J. Phys. Chem.* **1994**, *98*, 6023−6029. (c) Cherepy, N. J.; Holzwarth, A.; Mathies, R. A. *Biochemistry* **1995**, *34*, 5288−5293.

(15) Johnson, C. K.; Rabinovitz, R. *Spectrochim. Acta* **1991**, *47A*, 1413−1421.

(16) Noguchi, T.; Furukawa, Y.; Tasumi, M. *Spectrochim. Acta* **1991**, *47A*, 1431−1440.

(17) (a) Wachtveitl, J.; Farchaus, J. W.; Das, R.; Lutz, M.; Robert, B.; Mattioli, T. A. *Biochemistry* **1993**, *32*, 12875−12886. (b) Mattioli, T. A.; Williams, J. C.; Allen, J. P.; Robert, B. *Biochemistry* **1994**, *33*, 1636−1643. (c) Jones, M. R.; Heer-Dawson, M.; Mattioli, T. A.; Hunter, C. N.; Robert, B. *FEBS Lett.* **1994**, *339*, 18−24. (d) Mattioli, T. A.; Lin, X.; Allen, J. P.; Williams, J. C. *Biochemistry* **1995**, *43*, 6142−6152.

(18) (a) Peloquin, J. M.; Bylina, E. J.; Youvan, D. C.; Bocian, D. F. *Biochemistry* **1990**, *29*, 8417−8424. (b) Peloquin, J. M.; Bylina, E. J.; Youvan, D. C.; Bocian, D. F. *Biochim. Biophys. Acta* **1991**, *1056*, 85−88. (c) Palaniappan, V.; Bocian, D. F. *Biochemistry* **1995**, *34*, 11106−11116. (d) Palaniappan, V.; Schenck, C. C.; Bocian, D. F. *J. Phys. Chem.* **1995**, *99*, 17049−17058.

(19) (a) Mäntele, W.; Nabedryk, E.; Tavitian, B. A.; Kreutz, W.; Breton, J. *FEBS Lett.* **1985**, *187*, 227−232. (b) Mäntele, W.; Wollenweber, A.; Nabedryk, E.; Breton, J. *Proc. Natl. Acad. Sci. U.S.A.* **1988**, *85*, 8468−8472. (c) Nabedryk, E.; Bagley, K. A.; Thibodeau, D. L.; Bauscher, M.; Mäntele, W.; Breton, J. *FEBS Lett.* **1990**, *266*, 59−62. (d) Heinerwadel, R.; Thibodeau, B.; Lenz, F.; Nabedryk, E.; Breton, J.; Kreutz, W.; Mäntele, W. *Biochemistry* **1992**, *31*, 5799−5808. (e) Breton, J.; Burie, J.-R.; Berthomieu, C.; Thibodeau, D. L.; Andranambinintsoa, S.; Dejonghe, D.; Berger, G.; Nabedryk, E. In ref 6, pp 155−162. (f) Heinerwadel, R.; Nabedryk, E.; Breton, J.; Kreutz, W.; Mäntele, W. In ref 6, pp 163−172. (g) Leonhard, M.; Mäntele, W. *Biochemistry* **1993**, *32*, 4532−4538.

(20) (a) Morita, E. H.; Hayashi, H.; Tasumi, M. *Chem. Lett.* **1991**, 1583−1586. (b) Morita, E. H.; Hayashi, H.; Tasumi, M. *Chem. Lett.* **1991**, 1853−1856. (c) Morita, E. H.; Hayashi, H.; Tasumi, M. *Biochim. Biophys. Acta* **1993**, *1142*, 146−154.

(21) (a) Gerwert, K.; Hess, B.; Michel, H.; Buchanan, S. *FEBS Lett.* **1988**, *232*, 303−307. (b) Buchanan, S.; Michel, H.; Gerwert, K. *Biochemistry* **1992**, *31*, 1314−1322.

(22) (a) Breton, J.; Nabedryk, E.; Wachtveitl, J.; Gray, K. A.; Oesterheldt, D. In ref 6, pp 141−153. (b) Nabedryk, E.; Robles, S. J.; Goldman, E.; Youvan, D. C.; Breton, J. *Biochemistry* **1992**, *31*, 10852−10858. (c) Nabedryk, E.; Allen, J. P.; Taguchi, A. K. W.; Williams, J. C. *Biochemistry* **1993**, *32*, 13879−13885.

(23) (a) Meech, S. R.; Hoff, A. J.; Wiersma, D. A. *Chem. Phys. Lett.* **1985**, *121*, 287−292. (b) Meech, S. R.; Hoff, A. J.; Wiersma, D. A. *Proc. Natl. Acad. Sci. U.S.A.* **1986**, *83*, 9464−9468.

(24) (a) Boxer, S. G.; Lockhart, D. J.; Middendorf, T. R. *Chem. Phys. Lett.* **1986**, *123*, 476−482. (b) Middendorf, T. R.; Mazzola, L. T.; Gaul, D. F.; Schenck, C. C.; Boxer, S. G. *J. Phys. Chem.* **1991**, *95*, 10142−10151.

(25) (a) Hayes, J. M.; Small, G. J. *J. Phys. Chem.* **1986**, *90*, 4928−4931. (b) Johnson, S. G.; Tang, D.; Jankowiak, R.; Hayes, J. M.; Small, G. J.; Tiede, D. M. *J. Phys. Chem.* **1989**, *93*, 5953−5957. (c) Johnson, S. G.; Tang, D.; Jankowiak, R.; Hayes, J. M.; Small, G. J.; Tiede, D. M. *J. Phys. Chem.* **1990**, *94*, 5849−5855. (d) Lyle, P. A.; Kolaczkowski, S. V.; Small, G. J. *J. Phys. Chem.* **1993**, *97*, 6924−6933. (e) Hayes, J. M.; Lyle, P. A.; Small, G. J. *J. Phys. Chem.* **1994**, *98*, 7337−7341.

(26) Klevanik, A. V.; Ganago, A. O.; Shkuropatov, A. Y.; Shuvalov, V. A. *FEBS Lett.* **1988**, *237*, 61−64.

which initiates the primary charge separation process in RCs. This strong coupling is absent for the monomeric cofactors in the RC. The hole-burning and optical data were interpreted in terms of only a few (one or two) strongly coupled modes. However, RR studies conducted with excitation into the near-infrared absorption feature due to P* have shown that the actual number of strongly coupled, very low-frequency modes is considerably larger (5−10).[13d,14,18d] More recently, femtosecond optical experiments on P* have shown that a number of very low-frequency vibrational modes undergo relatively long-lived (picosecond) coherent oscillations upon excitation of the photophysically important state.[27,28] At this time, the identity of these strongly coupled, low-frequency vibrations is not certain. It is also not certain whether these modes play any role in mediating the initial electron-transfer events in RCs or ride along as spectators.

The uncertain identity of the strongly coupled, low-frequency modes of P makes it difficult to gain a clear sense of their potential importance for modulating the electron-transfer dynamics in RCs. The only reliable way of determining the identity of any vibrational mode is via examination of isotopically labeled species. Toward this end, we undertook a detailed low-frequency (50−425-cm^{-1}) RR study of RCs in which the BChl and BPh cofactors are labeled with ^{15}N or ^{26}Mg. The focus of the study is the identification of the strongly coupled, very low-frequency modes of P which are observed with excitation into the near-infrared absorption feature of the dimer. Previous RR studies of isotopically labeled RCs have focused primarily on the high-frequency vibrational modes of the BChl and BPh cofactors.[11a] In addition, these studies have used excitation into the higher lying B- or Q_x-excited states of the cofactors rather than the lowest energy, photophysically important state(s). In order to gain a complete picture of the effects of isotopic substitution on the low-frequency vibrational characteristics of the cofactors, the near-infrared-excitation RR spectra of the accessory BChls and the BPhs in the RCs were examined in addition to those of P. The RR spectra of the isotopically labeled cofactors in the RCs were compared with one another and with the spectra obtained for solid-film samples of isolated, isotopically labeled BChl and BPh. Based on these comparisons and the predictions of semiempirical normal coordinate calculations, a self-consistent set of assignments has been developed for all the RR active modes of the different BChl and BPh cofactors in the RC which are observed in the very low-frequency regime (50−250 cm^{-1}). These assignments provide insights into the structural characteristics of P which give rise to strong coupling of certain types of vibrational modes. The assignments also serve as benchmarks for the interpretation of the vibrational coherences observed in ultrafast spectra and provide information necessary for the construction of more complete vibronic models of electron transfer in RCs.

The organization of the paper is as follows: First, we present the results of the RR studies and summarize the vibrational assignments. Next, we discuss the effects of isotopic substitution on the RR spectra. We then describe our general approach for obtaining a self-consistent set of vibrational assignments and the assignments for the modes of the different cofactors. Finally, we discuss the strong coupling of specific low-frequency modes of P in the context of the structure of the dimer and how motions along these coordinates could modulate the physicochemical properties of the primary electron donor.

Materials and Methods

Sample Preparation. *Rb. sphaeroides* 2.4.1 was grown in a modified Hunter's (minimal) medium.[29] The RCs were isolated and purified as previously described.[30] All proteins were eluted from a DEAE anion-exchange column by using 0.01 M Tris (pH 8.0), 0.15% Triton X-100, and 0.5 M NaCl. The chemically reduced RCs used for the RR experiments were prepared by adding a slight excess of $Na_2S_2O_4$.

The incorporation of ^{26}Mg was accomplished by substituting $^{26}MgSO_4$ for the naturally abundant material in the growth medium. ^{26}Mg was obtained as ^{26}MgO (^{26}Mg, 99.56%) from Isotec (Miamisburg, OH) and converted to $^{26}MgSO_4$ by dissolving in a slight stoichiometric excess of H_2SO_4 followed by evaporation to dryness. The incorporation of ^{15}N was accomplished by substituting $^{15}NH_4OOCCH_3$ (^{15}N, 98%+), obtained from Cambridge Isotopes (Andover, MA), for the naturally abundant material. The growth medium for the bacteria also contains caseamino acids as a nutrient source. This results in specific ^{15}N labeling of the BChl and BPh cofactors rather than universal ^{15}N labeling of the cofactors and protein. The isotopic purity of both the ^{26}Mg- and ^{15}N-labeled RCs was judged to be >95% based on the characteristics of the RR spectra (vide infra).

Natural abundance BChl was obtained commercially (Sigma, St. Louis, MO). [$^{15}N_4$]BChl and [^{26}Mg]BChl were extracted from the isotopically labeled whole cells. All extraction and purification procedures were conducted in a cold room under red light. BChl was extracted by shaking wet-packed cells (7.5 g in 20 mL of H_2O) with methanol (170 mL) followed by repeated extractions with petroleum ether. The extract was dried over anhydrous Na_2SO_4, filtered, and evaporated to dryness using a rotary evaporator. BChl was purified on a DEAE Sephacel column via elution with acetone of material dissolved in a minimal volume of acetone containing 1% methanol. The solvent was evaporated, and the BChl was redissolved in a minimal amount of methanol and loaded onto a 20 cm × 20 cm silica gel 60F plate. The plate was eluted with a mixture of 90% toluene/10% acetone. The band containing BChl was removed from the plate, dissolved in methanol, filtered, evaporated to dryness under nitrogen, and stored at low temperature. Natural abundance BPh and [$^{15}N_4$]BPh were prepared from the respective BChl sample by the addition of glacial acetic acid followed by the evaporation of the excess acid *in vacuo*. The products were separated on a DEAE Sepharose CL-6B column (20% ethanol (aqueous)) with acetone elution. The purity of all the BChl and BPh samples was verified by UV−vis spectroscopy.

RR Spectroscopy. The RR measurements on the RCs were made on optically dense, snowy samples contained in 1 mm i.d. capillary tubes. The advantages and disadvantages of using snowy versus glassy samples have been previously discussed.[18d] The RR measurements on the isolated pigments were made on optically dense, thin films deposited directly onto the cold tip (from a CCl_4 solution) of the refrigeration system as previously described.[31] The RR spectra of both the RCs and films were recorded at 25 K. Temperature control was maintained with a closed cycle liquid He refrigeration system (ADP Cryogenics, DE-202 Displex). The RR data were acquired at low temperature to minimize line broadening which might arise from anharmonicity effects in conjunction with thermal population of the higher vibrational states of the low-frequency modes. Although these line-broadening effects are expected to be small,[13d] the ^{15}N and ^{26}Mg isotope shifts are also relatively small (1−2 cm^{-1}) (vide infra), and even modest line broadening could interfere with the measurements.

The RR spectra were acquired with a red-optimized triple spectrograph and detection system that has been previously described.[13d,f]

(27) (a) Vos, M. H.; Lambry, J.-C.; Robles, S. J.; Youvan, D. C.; Breton, J.; Martin, J.-L. *Proc. Natl. Acad. Sci. U.S.A.* **1991**, *88*, 8885−8889. (b) Vos, M. H.; Lambry, J.-C.; Robles, S. J.; Youvan, D. C.; Breton, J.; Martin, J.-L. *Proc. Natl. Acad. Sci. U.S.A.* **1992**, *898*, 613−617. (c) Vos, M. H.; Rappport, F.; Lambry, J.-C.; Breton, J.; Martin, J.-L. *Nature* **1993**, *363*, 320−325. (d) Vos, M. H.; Jones, M. R.; Hunter, C. N.; Breton, J.; Lambry, J.-C.; Martin, J.-L. *Biochemistry* **1994**, *33*, 6750−6757. (e) Vos, M. H.; Jones, M. R.; McGlynn, P.; Hunter, C. N.; Breton, J.; Martin, J.-L. *Biochim. Biophys. Acta* **1994**, *1186*, 117−122. (f) Vos, M. H.; Jones, M. R.; Hunter, C. N.; Breton, J.; Lambry, J.-C.; Martin, J.-L. *Proc. Natl. Acad. Sci. U.S.A* **1994**, *91*, 12701−12705.

(28) Stanley, R. J.; Boxer, S. G. *J. Phys. Chem.* **1995**, *99*, 859−863.

(29) Cohen-Bazire, G.; Sistrom, W. R.; Stanier, R. Y. *J. Cell. Comp. Physiol.* **1957**, *49*, 25−68.

(30) McGann, W. J.; Frank, H. A. *Biochim. Biophys. Acta* **1985**, *807*, 101−109.

(31) (a) Diers, J. R.; Bocian, D. F. *J. Am. Chem. Soc.* **1995**, *117*, 6629−6630. (b) Diers, J. R.; Zhu, Y.; Blankenship, R. E.; Bocian, D. F. *J. Phys. Chem.* **1996**, *100*, 8573−8579.

A Ti:sapphire laser (Coherent 890), pumped by an Ar ion laser (Coherent Innova 400-15UV), or the discrete outputs of a Kr ion laser (Coherent Innova 200-K3) served as the excitation source. The laser powers were typically in the 0.3−1 mW range for the experiments on the RCs and ∼5 mW for those on the isolated pigments. In the case of the RCs, the power density was further lowered by defocusing the incident beam. The resulting photon fluxes (∼100 photons s^{-1} RC^{-1}) were sufficiently low that only a few percent of the RCs exist in photogenerated transient states. For the accessory BChls and the BPhs in the RCs and the solid-film samples of both types of isolated pigments, individual spectra were typically generated with 2 h of signal averaging (120 × 60 s scans). For P, the individual spectra were typically generated with 3.5 h of signal averaging (420 × 30 s scans). Cosmic spikes in the individual scans were removed prior to addition of the data sets. The spectral resolution was ∼2 cm^{-1} at a Raman shift of 200 cm^{-1}. The spectral data were calibrated using the known frequencies of fenchone.[32]

Isotope-Shift Measurements. Owing to the relatively small magnitude of the ^{15}N and ^{26}Mg isotope shifts, the sample and experimental conditions were carefully controlled to obtain reliable data. As a first step, the solution concentrations of the different isotopomers were adjusted to be identical (as judged by absorption spectroscopy) prior to addition to the capillary tube (RCs) or deposition on the cold tip (films). Next, the RR spectra obtained with a particular excitation wavelength were acquired by successive data accumulations on each of the different isotopomers, all of which were simultaneously mounted on the cold tip and spatially separated by ∼1 mm. After data accumulation on a given isotopomer, the next isotopomer was shifted into the laser beam via adjustment of a micrometer-driven positioner which holds the cryostat. This permitted data acquisition on the different isotopomers with no readjustment of the spectrometer or laser (except for occasional reoptimization of laser power needed to compensate for drift in very long experiments). The third step to insure the reliability of the isotopic-shift data was the acquisition of spectra for a number of independent samples. These latter studies showed that data obtained in the isotope-difference experiments were in all cases reproducible (the film samples are an exception (vide infra)).

Perhaps the most critical issue in accurately measuring the small ^{26}Mg and ^{15}N isotope shifts is the potential interference from fluorescence (either spurious or intrinsic).[13,14,18] Previous near-infrared-excitation RR studies on RCs have shown that the low-frequency RR scattering from P occurs in a spectral window where the fluorescence is substantial and much larger than the RR signals.[13c,d,14,18d] The present studies indicate that this situation also applies to the BPhs in the RCs (vide infra). In contrast, the low-frequency RR scattering from the accessory BChls falls in a region where the emission is minimal and the RR signals are clearly visible above the background.[18d] This is also the case for thin films of isolated BChl[31d] and BPh (vide infra).

The large fluorescence background underlying the RR spectra of P and the BPhs in the RCs precludes the determination of the isotope shifts via conventional techniques, such as simple isotope-difference methods. As a consequence, the isotope shifts for these cofactors were obtained exclusively using double-difference techniques. The double-difference measurement is a combination of the shifted excitation Raman difference spectroscopic (SERDS) method[14,33] and a conventional isotope-difference experiment. The SERDS method and its application to RR studies of RCs have been previously described in detail.[14,33,18d] Briefly, data sets are acquired at two excitation wavelengths which differ by a small wavenumber increment (typically 10 cm^{-1}). These data sets are subtracted to yield a RR difference spectrum which is free from background interference. In the standard experiment, the normal RR spectrum is then reconstructed from the SERDS data by fitting the latter to a series of derivative-shaped functions (in our case, difference bands generated from Gaussian or voigt functions) of arbitrary frequency, amplitude, and width.

The first step in the double-difference experiment is to acquire SERDS data for each of the isotopomers. The SERDS data presented herein were obtained by subtracting the initial spectrum from the shifted spectrum. The spectral window is defined by the initial spectrum and corresponds to the wavenumber axis shown in the figures. The experiments were conducted via successive acquisition of the RR spectrum of each isotopomer at a given excitation wavelength followed by a shift in the excitation wavelength and the reacquisition of the spectrum of each isotopomer. The SERDS data were then generated for each isotopomer. In order to check the precision of the method, additional SERDS data sets were generated by varying the order of spectral acquisition among the isotopomers. These different SERDS data sets were found to be identical.

The double-difference spectra were generated by subtracting the raw SERDS data obtained for the labeled sample from that obtained for the natural abundance sample. In these spectra, the isotopically shifted bands give rise to features which have the qualitative appearance of second derivatives. However, the exact appearance of each spectral feature is determined by the convolution of the excitation-wavelength shift and isotope shift. Modes which do not undergo isotope shifts are nulled as is the case for the standard isotope-difference experiment. The final step in determining the isotope shifts was to fit the features in the double-difference spectrum to differences between SERDS-like features. The SERDS-like features used in the simulations were obtained by subtracting two line shape functions (Gaussian or voigt) of identical height and width which were displaced from one another by the excitation-wavelength shift used in the SERDS experiment. After a satisfactory fit was obtained to the double-difference spectrum, the conventional isotope-difference spectrum was reconstructed.

For an alternative assessment of the isotope shifts, the normal RR spectrum of each isotopomer was first reconstructed from the SERDS data and conventional isotope-difference spectra were then obtained by subtracting the reconstructed spectra. This method yielded reasonable results as judged by the appearance of nearly symmetrical derivative-like features for isotope-sensitive features and approximate nulling of the signals of unshifted bands. In general, the isotope-difference spectra obtained by this latter method were found to be essentially identical with those obtained via the true double-difference method. Regardless, the true double-difference method should be intrinsically more accurate because no data manipulation is performed between spectral subtractions. Accordingly, all of the reconstructed isotope-difference spectra shown in the figures were obtained via the true double-difference method.

The absence of a significant emission background in the RR spectra of the accessory BChls in the RCs and the thin films of both BChl and BPh in principle permits isotope shifts to be obtained via standard difference techniques. In the case of the accessory BChls, this method yielded satisfactory results as judged by the appearance of nearly symmetrical derivative-like features for isotope-sensitive features and essential nulling of the signals of unshifted bands (vide infra). In contrast, the isotope-difference experiments conducted on the thin films of both BChl and BPh yielded unsatisfactory results. In attempts to obtain a more accurate assessment of the isotope shifts for the film samples, double-difference spectra were also acquired. Although this latter method yielded more reliable difference data than the conventional technique, the sample-to-sample variations in the double-difference data for the films were much larger than those observed for the RCs. As a consequence, the fits to the film data were inferior to those obtained for the proteins. Although isotope-sensitive RR bands could be identified for the film samples, values for the isotope shifts could not be accurately determined. The greater variability in the difference data for the films is attributed to heterogenities which occur during the deposition process.

One final note concerns the accuracy of the isotope shifts determined from the fits to the difference spectra of the RCs. As was previously noted, the magnitudes of both the ^{15}N and ^{26}Mg shifts are relatively small (<2 cm^{-1}). These shifts are also much smaller than the line widths of the RR bands (∼10 cm^{-1}). As a consequence, the line width parameter used in the simulations of the difference data has some influence on the magnitude of the isotope shift determined from the fit. Based on simulations conducted using a variety of parameters, all of which give reasonable fits to the difference spectra, the accuracy of the isotope shifts was estimated to be on the order of ±0.5 cm^{-1}. Accordingly, the calculated shifts listed in the tables are rounded to the nearest wavenumber.

(32) Yu, N.-T.; Srivastava, R. B. *J. Raman Spectrosc.* **1980**, *9*, 166−171.

(33) Shreve, A. P.; Cherepy, N. J.; Mathies, R. A. *Appl. Spectrosc.* **1992**, *46*, 707−711.

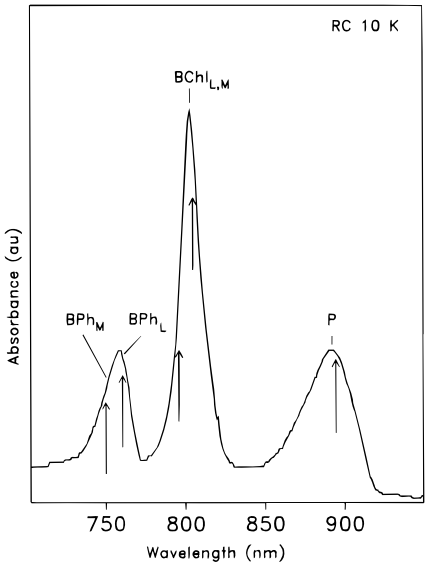

Figure 3. Low-temperature (10 K) near-infrared absorption spectrum of RCs from *Rb. sphaeroides*. The cofactors contributing to the various absorptions are indicated. The arrows mark the different excitation wavelengths used to acquire RR spectra.

Normal Coordinate Calculations. The vibrational frequencies and eigenvectors for the low-frequency modes of BChl and BPh were calculated using the QCFF/PI method.[34] The calculations were conducted as described in our earlier studies of the low-frequency modes of BChl.[13d] However, in the present analysis, imidazole was explicitly included as an axial ligand. The σ-bond parameters for the Mg(II)−imidazole bond were adjusted such that the optimized bond length reproduced the average of the Mg(II)−histidine bond lengths observed for the accessory BChls and BChls in P (∼2.25 Å) in the X-ray crystal structure of *Rb. sphaeroides* reported by Ermler et al.[8d] The standard parameters available in the QCFF/PI program were used for BPh.

Results

The near-infrared region of the low-temperature (10 K) absorption spectrum of RCs from *Rb. sphaeroides* is shown in Figure 3. The principal contributors to the different absorption bands are indicated in the figure. The various exciting lines used to probe the RCs are indicated by the arrows.

The low-frequency region of the near-infrared-excitation (λ_{ex} = 894 nm) RR spectrum of P in the RCs is shown in Figure 4. The top three traces are the SERDS data for the natural abundance (NA), ^{26}Mg-labeled, and ^{15}N-labeled RCs, respectively. The fourth and fifth traces are the double-difference spectra (NA SERDS − ^{26}Mg or ^{15}N SERDS). The sixth and seventh traces are the fitted double-difference spectra. The eighth and ninth traces are the ^{26}Mg and ^{15}N isotope-difference spectra reconstructed from the double-difference data. For clarity, the fits of the individual SERDS traces are not shown in the figure. We have previously presented both observed and fitted SERDS data for P recorded at 200 K.[18d] The data obtained at 25 K are essentially identical except for small frequency shifts and the narrowing of certain bands. However, the line narrowing does permit the identification of a few additional features. The bottom trace in Figure 4 is the RR spectrum of the NA RCs which was reconstructed from the fitted SERDS data. In this spectrum, the bands sensitive to ^{26}Mg substitution are labeled in bold, the bands sensitive to ^{15}N substitution are labeled in italics, and the bands sensitive to both isotopic substitutions are labeled in bold-italics.

(34) (a) Warshel, A.; Karplus, M. *J. Am. Chem. Soc.* **1972**, *94*, 5612−5625. (b) Warshel, A.; Levitt, M. *Quantum Chemistry Program Exchange*, No. 247; Indiana University, 1974.

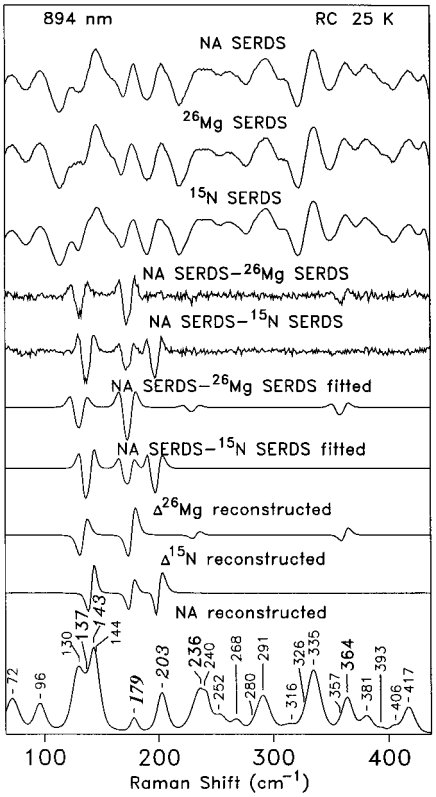

Figure 4. Low-frequency region of the near-infrared-excitation (λ_{ex} = 894 nm) RR spectrum of P in the RCs. The top three traces are the SERDS data for the NA, ^{26}Mg-labeled, and ^{15}N-labeled RCs, respectively. The fourth and fifth traces are the double-difference spectra (NA SERDS − ^{26}Mg or ^{15}N SERDS). The sixth and seventh traces are the fitted double-difference spectra. The eighth and ninth traces are the ^{26}Mg and ^{15}N isotope-difference spectra reconstructed from the double-difference data. The bottom trace is the RR spectrum of the NA RCs which was reconstructed from the SERDS data. The bands sensitive to ^{26}Mg substitution are labeled in bold; the bands sensitive to ^{15}N substitution are labeled in italics; the bands sensitive to both isotopic substitutions are labeled in bold-italics.

The low-frequency region of the near-infrared-excitation (λ_{ex} = 805 nm) RR spectrum of the accessory BChls in the RCs is shown in Figure 5. Spectra were also obtained with λ_{ex} = 796 nm (not shown); however, these spectra were essentially identical with those shown. The top three traces in Figure 5 are the normal RR spectra of the NA, ^{26}Mg-labeled, and ^{15}N-labeled RCs, respectively. The bands sensitive to ^{26}Mg substitution are labeled in bold, the bands sensitive to ^{15}N substitution are labeled in italics, and the bands sensitive to both isotopic substitutions are labeled in bold-italics. The fourth and fifth traces are the observed and fitted isotope-difference spectra for the ^{26}Mg-labeled RCs. The sixth and seventh traces are the observed and fitted isotope-difference spectra for the ^{15}N-labeled RCs.

The low-frequency regions of the near-infrared-excitation RR spectra of BPh$_L$ (λ_{ex} = 760 nm) and BPh$_M$ (λ_{ex} = 750 nm) in the RCs are shown in Figures 6 and 7, respectively. As far as we know, low-frequency, near-infrared-excitation RR spectra of the BPhs have not been previously reported. In each figure, the top two traces are the SERDS data for the NA and ^{15}N-labeled RCs, respectively. The third and fourth traces are fits of the SERDS data. The fifth trace is the double-difference spectrum (NA SERDS − ^{15}N SERDS). The sixth trace is the fitted double-difference spectrum. The seventh trace is the ^{15}N isotope-difference spectrum reconstructed from the double-difference data. The bottom trace is the RR spectrum of the NA RCs which was reconstructed from the fitted SERDS data.

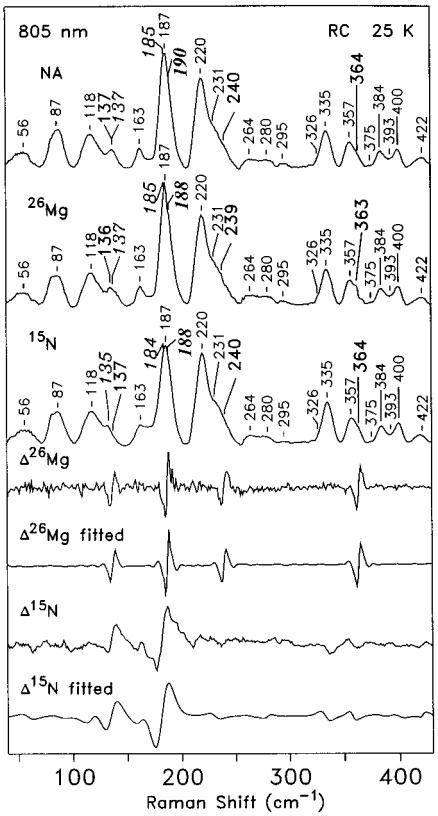

Figure 5. Low-frequency region of the near-infrared-excitation (λ_{ex} = 805 nm) RR spectrum of the accessory BChls in the RCs. The top three traces are the normal RR spectra of the NA, ^{26}Mg-labeled, and ^{15}N-labeled RCs, respectively. The bands sensitive to ^{26}Mg substitution are labeled in bold; the bands sensitive to ^{15}N substitution are labeled in italics; the bands sensitive to both isotopic substitutions are labeled in bold-italics. The fourth and fifth traces are the observed and fitted isotope-difference spectra for the ^{26}Mg-labeled RCs. The sixth and seventh traces are the observed and fitted isotope-difference spectra for the ^{15}N-labeled RCs.

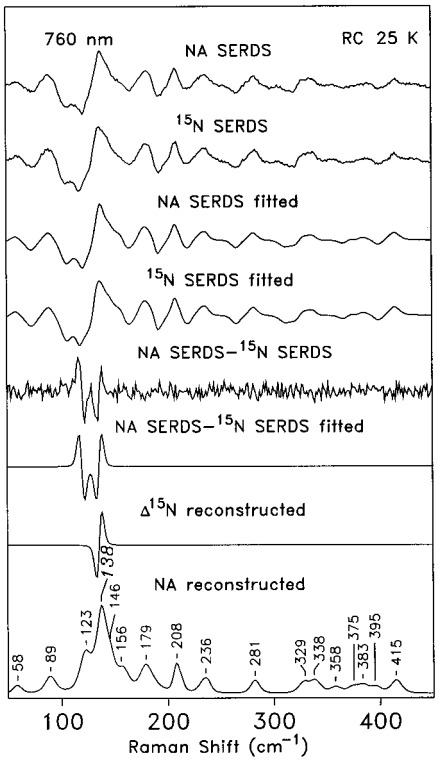

Figure 6. Low-frequency region of the near-infrared-excitation (λ_{ex} = 760 nm) RR spectrum of BPh_L in the RCs. The top two traces are the SERDS data for the NA and ^{15}N-labeled RCs, respectively. The third and fourth traces are fits of the SERDS data. The fifth trace is the double-difference spectrum (NA SERDS − ^{15}N SERDS). The sixth trace is the fitted double-difference spectrum. The seventh trace is the ^{15}N isotope-difference spectrum reconstructed from the double-difference data. The bottom trace is the RR spectrum of the NA RCs which was reconstructed from the SERDS data. The bands sensitive to ^{15}N substitution are labeled in italics.

In this spectrum, the bands sensitive to ^{15}N substitution are labeled in italics.

In order to facilitate comparison of the RR spectra of the BChls and BPhs, the conventional RR spectra (either directly obtained or reconstructed) with the isotope-sensitive modes marked are reproduced in Figures 8 and 9, respectively. The low-frequency regions of the near-infrared-excitation RR spectra of the thin-film samples of NA BChl (λ_{ex} = 800 nm) and NA BPh (λ_{ex} = 750 nm) are included in these two figures. The RR spectra shown for the films were obtained by standard (rather than SERDS) techniques.

The frequencies and isotope shifts observed for the low-frequency RR bands of the BChls in the RCs and films are listed in Table 1. The spectral data obtained for the BPhs are summarized in Table 2. In the tables, the ^{26}Mg and ^{15}N shifts are indicated in parentheses and brackets, respectively. In the case of the BChl and BPh films, the isotope-sensitive mode(s) are designated by "s" because the poorer quality of the spectral data does not permit determination of reliable values (vide supra). In Table 1, the bands observed for P are designated by P_L because previous near-infrared-excitation RR studies of RCs have shown that only the BChl cofactor of P in the L subunit contributes to the RR scattering.[18d] The bands observed for the accessory BChls are designated by $BChl_{L,M}$ because both cofactors contribute to the RR spectra obtained with λ_{ex} = 795−805 nm. However, only a single set of frequencies is listed for $BChl_{L,M}$ in Table 1 because the RR spectra of the two cofactors are essentially identical.[14c,18d] This is not the case for BPh_L and BPh_M; hence the frequencies for these cofactors are listed separately in Table 2. Finally, it should be noted that the correlations between certain of the low-frequency modes of P_L, $BChl_{L,M}$, and $BChl_{film}$ are somewhat different than those we have previously proposed.[18d] The revised correlations incorporate the new information obtained from the studies of the isotopically substituted systems.

The calculated frequencies, ^{26}Mg and ^{15}N isotope shifts, and normal mode descriptions for the very low-frequency (<250-cm^{-1}) vibrations of BChl and BPh are listed in Table 3. A proposed set of vibrational assignments for the RR active modes of the BChls and BPhs in the RCs and films is also included in the table. The table also correlates the modes of BChl and BPh whose calculated vibrational eigenvectors are very similar.

Discussion

Effects of Isotopic Substitution. Inspection of the RR data reveals that relatively few modes of BChl and BPh undergo ^{15}N and ^{26}Mg isotope shifts. This result is consistent with the fact that the isotopic labels are confined to a localized region in the core of the BChl and BPh macrocycles and is predicted by the normal coordinate calculations (vide infra). The majority of the isotope-sensitive bands occur in the 130−250-cm^{-1} region. No shifts are observed for bands below 100 cm^{-1}, and only a single isotope-sensitive band is observed in the 250−425-cm^{-1} region. Bands other than those marked may also exhibit some isotope sensitivity; however, the shifts are so small that they cannot be reliably identified. In the following sections,

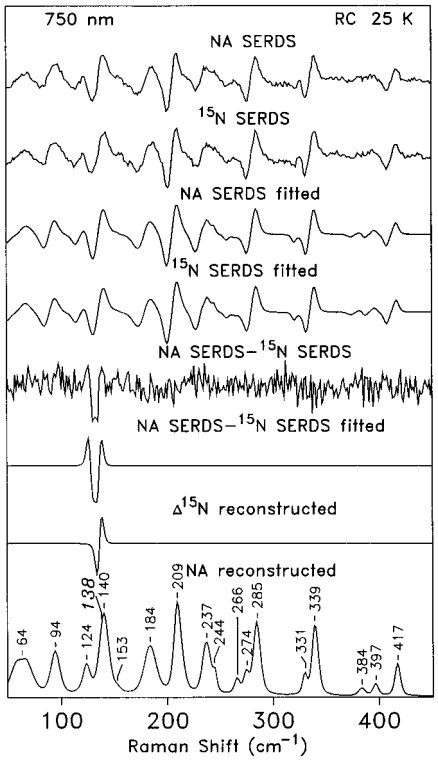

Figure 7. Low-frequency region of the near-infrared-excitation (λ_{ex} = 750 nm) RR spectrum of BPh_M in the RCs. The top two traces are the SERDS data for the NA and ^{15}N-labeled RCs, respectively. The third and fourth traces are fits of the SERDS data. The fifth trace is the double-difference spectrum (NA SERDS − ^{15}N SERDS). The sixth trace is the fitted double-difference spectrum. The seventh trace is the ^{15}N isotope-difference spectrum reconstructed from the double-difference data. The bottom trace is the RR spectrum of the NA RCs which was reconstructed from the SERDS data. The bands sensitive to ^{15}N substitution are labeled in italics.

we discuss the effects of isotopic substitution on the RR spectral features of the BChls and BPhs in the RCs and films in more detail.

1. Special Pair BChl (P_L). P_L exhibits RR bands sensitive to ^{26}Mg substitution at 137, 236, and 364 cm^{-1}. Bands sensitive to ^{15}N substitution are observed at 143 and 203 cm^{-1}. The RR band at 179 cm^{-1} is sensitive to both ^{26}Mg and ^{15}N substitution. The ^{26}Mg-sensitive band at 137 cm^{-1} merits additional comment. In the RR spectrum, no band is clearly observed at this wavenumber (Figures 4 and 8). Instead, only two clear features are observed at 130 and 143 cm^{-1}. The feature which appears in the ^{26}Mg difference spectrum cannot be associated with either the 130- or 143-cm^{-1} bands. In order to adequately fit both the SERDS data and the isotope-difference data, the 130-cm^{-1} band must be included as an isotope-insensitive feature and a new, ^{26}Mg-sensitive band must be included near 137 cm^{-1}. This band fills in the gap between the 130-cm^{-1} band and the ^{15}N-sensitive band at 143 cm^{-1}. The spectral simulations indicate that the intensity of the 137-cm^{-1} band is comparable to that of the 130-cm^{-1} band. The simulations of the ^{15}N SERDS data further indicate that a weaker, isotope-insensitive feature is present near 144 cm^{-1}. This band is revealed in the spectrum of the ^{15}N-substituted RCs owing to the downshift of the 143-cm^{-1} band. It should be noted that the isotope-insensitive 144-cm^{-1} band cannot be attributed to the presence of a small fraction of unlabeled RCs. This is evidenced by the fact that no residual features are observed in the region of the 203-cm^{-1} band which is also sensitive to ^{15}N substitution. Finally, it should be noted that neither the 137- nor 144-cm^{-1} bands of P_L have been previously identified.[13d,14,18d] The identification

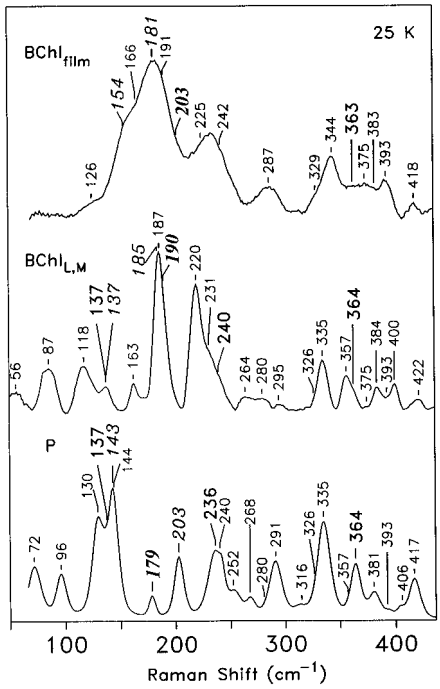

Figure 8. Comparison of the low-frequency regions of the near-infrared-excitation RR spectra of P (bottom trace), the accessory BChls (middle trace), and the BChl film (top trace). The bands sensitive to ^{26}Mg substitution are labeled in bold; the bands sensitive to ^{15}N substitution are labeled in italics; the bands sensitive to both isotopic substitutions are labeled in bold-italics.

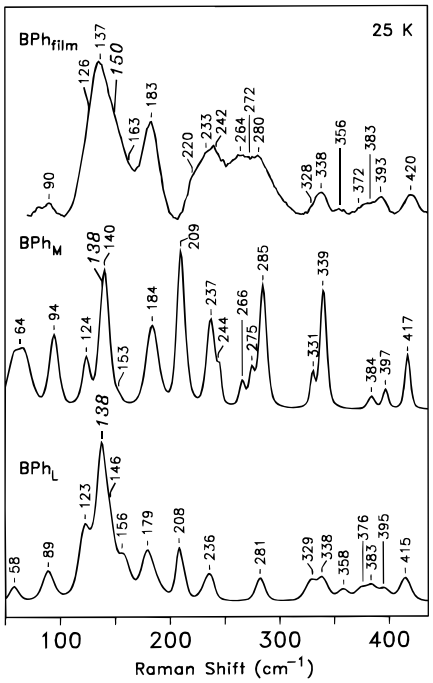

Figure 9. Comparison of the low-frequency regions of the near-infrared-excitation RR spectra of BPh_L (bottom trace), BPh_M (middle trace), and the BPh film (top trace). The bands sensitive to ^{15}N substitution are labeled in italics.

of these modes in the isotopically substituted RCs exemplifies the utility of isotope labeling for revealing the true characteristics of congested spectra which contain overlapping features.

2. Accessory BChls ($BChl_{L,M}$). $BChl_{L,M}$ exhibits RR bands sensitive to ^{26}Mg substitution at 137, 240, and 364 cm^{-1}. Bands sensitive to ^{15}N substitution are observed at 137 and 185 cm^{-1}. The RR band at 190 cm^{-1} is sensitive to both ^{26}Mg and ^{15}N substitution. The 137-cm^{-1} feature arises from two overlapped

Table 1. Frequencies and Isotope Shifts (cm^{-1}) for Low-Frequency (<425-cm^{-1}) Modes of BChl in RCs and Films Observed with Near-Infrared Excitation[a]

P_L	$BChl_{L,M}$	$BChl_{film}$
72	56	
96	87	90[b]
130	118	126
137(2)[c]	137(1)	
143[2]	137[2]	154[s]
144	163	166
203[2]	185[1]	181[s]
	187	191
179(2)[1]	190(2)[2]	203(s)[s]
240	220	225
252	231	242
236(<1)	240(1)	
268	264	259[b]
280	280	287
291	295	
316		
326	326	329
335	335	344
357	357	359[b]
364(<1)	364(1)	363(s)
	375	375
381	384	383
393	393	393
406	400	405[b]

[a] P_L, $\lambda_{ex} = 894$ nm; $BChl_{L,M}$, $\lambda_{ex} = 805$ nm; $BChl_{film}$, $\lambda_{ex} = 800$ nm. [b] Observed at $\lambda_{ex} = 750$ nm (ref 31a). [c] Fitted (^{26}Mg) and [^{15}N] isotope shifts. For the $BChl_{film}$, the modes sensitive to isotopic substitution are indicated by "s".

Table 2. Frequencies and Isotope Shifts (cm^{-1}) for Low-Frequency (<425-cm^{-1}) Modes of BPh in RCs and Films Observed with Near-Infrared Excitation[a]

BPh_L	BPh_M	BPh_{film}
58	64	
89	94	90
123	124	126
138(2)[b]	138(2)	150(s)
146	140	137
156	153	163
179	184	183
208	209	220
236	237	233
	244	243
	266	264
	274	272
281	285	280
329	331	328
338	339	338
358		356
375		372
383	384	383
395	397	393
415	417	420

[a] BPh_L, $\lambda_{ex} = 760$ nm; BPh_M, $\lambda_{ex} = 750$ nm; BPh_{film}, $\lambda_{ex} = 750$ nm. [b] Fitted [^{15}N] isotope shifts. For the BPh_{film}, the modes sensitive to isotopic substitution are indicated by "s".

bands, one ^{15}N sensitive and the other ^{26}Mg sensitive, rather than a single band sensitive to both isotopic substitutions as is evidenced by changes in the shape of the band in the spectra of the different isotopomers. It should also be noted that the ^{15}N isotope-difference spectrum exhibits certain features which qualitatively appear to be shifted bands but which are not labeled as such (Figure 5, sixth trace). These features are actually due to slight intensity differences between the spectra and are quantitatively reproduced as such (for example, the feature near 340 cm^{-1}; Figure 5, bottom trace).

Comparison of the RR spectra of $BChl_{L,M}$ with those of P_L reveals that both the number of isotope-sensitive bands and the pattern of the isotope shifts are identical for the different cofactors in the RCs (Figure 8). This permits a one-to-one correlation of the isotope-sensitive features of these pigments (Table 1). In general, the frequencies of the isotope-sensitive modes of $BChl_{L,M}$ and P_L are also similar. The largest difference is ~18 cm^{-1} which occurs in the mode of $BChl_{L,M}$ at 185 cm^{-1} versus its analog in P_L at 203 cm^{-1}. The frequency differences observed between the isotope-sensitive modes of $BChl_{L,M}$ and P_L (and between modes which are not isotope sensitive) are attributed to structural differences between the cofactors, as has been previously discussed in detail.[13f,18c,d]

The most striking difference between the isotope-sensitive spectral features of $BChl_{L,M}$ versus P_L is in the relative intensities of certain modes. In particular, for $BChl_{L,M}$, the 137-cm^{-1} feature, attributed to two overlapped ^{26}Mg- and ^{15}N-sensitive (respectively) bands, is very weak. [In previous near-infrared-excitation RR studies of RCs, which were conducted at higher temperature, this feature is barely discernible and could not be clearly identified as a band (ref 18d, Figure 5).] The weakness of these features can be contrasted with the significant intensity of the analog modes of P_L observed at 137 and 143 cm^{-1}, respectively. Conversely, $BChl_{L,M}$ exhibits a strong feature centered near 187 cm^{-1}, whereas P_L exhibits a relatively weak feature near 179 cm^{-1}. The isotopic substitution studies reveal that the 187-cm^{-1} feature of $BChl_{L,M}$ is due to the overlap of three bands: a strong feature near 185 cm^{-1} sensitive to ^{15}N substitution, a second strong feature near 190 cm^{-1} sensitive to both ^{15}N and ^{26}Mg substitution, and a third somewhat weaker feature near 187 cm^{-1} which is isotope insensitive. For P_L, the analog bands are shifted further apart and do not overlap. In particular, the 185- and 190-cm^{-1} bands of $BChl_{L,M}$ correspond to the 203- and 179-cm^{-1} bands of P_L, respectively. The P_L analog of the 187-cm^{-1} isotope-insensitive mode of $BChl_{L,M}$ is not observed. Unlike the very low-frequency modes, the frequencies and relative intensities of the higher frequency, isotope-sensitive modes of $BChl_{L,M}$ and P_L (near 240 and 364 cm^{-1}) are quite similar.

3. $BChl_{film}$. $BChl_{film}$ exhibits a RR band sensitive to ^{26}Mg substitution at 363 cm^{-1}. Bands sensitive to ^{15}N substitution are observed at 154 and 181 cm^{-1}. The RR band near 203 cm^{-1} is sensitive to both ^{26}Mg and ^{15}N substitution. Both the frequencies and isotope shifts of these RR bands of the film are similar to those observed for bands of P_L and $BChl_{L,M}$ (Figure 8, Table 1). The most significant difference between the RR spectra of BChl in the film versus RCs is the absence of ^{26}Mg-sensitive modes near 137 and 240 cm^{-1}. Owing to the breadth of the RR bands of $BChl_{film}$, it is not possible to ascertain whether these bands are truly absent from the spectrum or present but very weak. The RR spectrum of $BChl_{film}$ also differs from that of the cofactors in the RCs in that the very low-frequency modes (<150 cm^{-1}) are either very weak or absent.

The spectral differences observed for BChl in the film versus RCs have been attributed primarily to structural differences in the pigment in the two environments.[31a] However, the detailed nature of these structural differences has not been elucidated. Nevertheless, one obvious structural difference between the film and protein is the nature of the axial ligand of the Mg(II) ion. For P_L and $BChl_{L,M}$, a histidine residue serves as the axial ligand.[8d,e] For $BChl_{film}$, the oxygen atom of a carbonyl group on a given pigment most likely serves as the axial ligand to the Mg(II) ion of an adjacent pigment. This would alter the vibrational characteristics of modes involving the Mg(II) ion (and the carbonyl substituents on the macrocycle) and could explain why certain ^{26}Mg-sensitive RR bands observed for P_L

Table 3. Vibrational Assignments and Correlations of Selected Low-Frequency Modes of BChl and BPh

description[a]	calcd BChl	obsd			calcd BPh	obsd		
		P_L	$BChl_{L,M}$	$BChl_{film}$		BPh_L	BPh_M	BPh_{film}
γC_2C_{acetyl}	30	36[b]	no[b,c]	*d*	30	*d*	*d*	*d*
$\gamma C_{acetyl}CH_3$, γC_bCH_3(I),	63	72	56	*d*	74	58	64	*d*
γC_bCH_3 (I), $\gamma C_{acetyl}CH_3$, γC_9=O	83	96	87	90	84	89	94	90
δC_2C_{acetyl}	131	130	118	126	121	123	124	126
γMg_{dome}	182(2.2)[e]	137(2)	137(1)	no	na	na	na	na
γrings I-IV(tilt, translation), γC_9=O, γC_b(I)CH_3	154[1.2]	143[2]	137[2]	154[s]	na	na	na	na
γrings III,IV (tilt, translation), γC_9=O	na	na	na	na	127[1.4]	138[2]	138[2]	150[s]
γring III (swivel), $\delta C_{10}C_{carbo}$	na	na	na	na	138	146	140	137
$\delta C_{acetyl}CH_3$, δC_bC_{alkyl}(II,IV)	160	144	163	166	153	156	153	163
δC_bC_{alkyl}(II,IV), $\delta C_{10}C_{carbo}$, δC_9=O	198	no	187	181	195	179	184	183
γMgN_{pyr} , δC_9=O, $\delta C_{10}C_{carbo}$	191(0.3)[0.5]	179(2)[1]	190(2)[2]	203(s)[s]	na	na	na	na
γrings I,II,IV (translation, swivel)	176[1.0]	203[2]	185[1]	181[s]	na	na	na	na
δC_bCH_3(I), δC_bC_{alkyl}(II, IV)	221	240	220	225	216	208	209	220
νMgN_{his}	232(1.6)	236(<1)	240(1)	na	na	na	na	na

[a] Mode descriptions are as follows: ν = stretch, δ = in-plane deformation, γ = out-of-plane deformation. The designators C_a, C_b, C_m, I−IV, α, β, γ, and δ refer to Figure 2. For a description of tilt, translation, and swivel, see ref 35. [b] Taken from ref 14. [c] Abrevations: no = not observed, na = no analogous normal mode. [d] This frequency regime could not be examined due to experimental limitations. [e] Calculated (^{26}Mg) and [^{15}N] isotope shifts. If no shift is indicated, its value is less than 0.5 cm^{-1}.

and $BChl_{L,M}$ are absent from the spectra of $BChl_{film}$. This assessment is borne out by the vibrational assignments discussed below.

4. BPh_L, BPh_M, and BPh_{film}. BPh_L, BPh_M, and BPh_{film} each exhibit a single ^{15}N-sensitive RR band in the 50−425-cm^{-1} region (Figure 9, Table 2). This band is observed near 138 cm^{-1} for both BPh_L and BPh_M and near 150 cm^{-1} for BPh_{film}. It should be emphasized that the frequency and isotope shift of the ^{15}N-sensitive RR band of BPh_L are essentially identical with those of the analogous band of BPh_M despite the fact that the shapes of the features in the double-difference spectra are qualitatively different. This difference arises because the excitation-wavelength shifts are different in the experiments conducted with λ_{ex} = 760 nm (BPh_L) versus λ_{ex} = 750 nm (BPh_M). [Recall that the appearance of the double-difference spectrum is determined by a convolution of the isotope shift and the excitation-wavelength shift (vide supra).] The other RR spectral features of the two BPh cofactors in the RCs are also qualitatively similar; however, the frequencies and relative intensities of certain RR bands are different. For example, BPh_L exhibits bands at 58, 89, 146, and 179 cm^{-1}, whereas the analogous bands of BPh_M occur at 64, 94, 140, and 184 cm^{-1}. The fact that these sets of modes are mutually exclusive with excitation at λ_{ex} = 760 nm versus λ_{ex} = 750 nm indicates that BPh_L and BPh_M can be probed quite selectively at these two excitation wavelengths. This result is somewhat unexpected owing to the relatively close energetic proximity of the Q_y bands of the two cofactors (Figure 3).

The spectral differences between BPh_L, BPh_M, and BPh_{film} are attributed to structural differences between the pigments in the different environments. In the case of RCs, X-ray crystallographic studies have shown that the structures of the two BPh cofactors are clearly different.[8d,e] High-frequency RR studies of RCs have shown that BPh modes involving motions in rings III and V exhibit frequencies most different between BPh_L and BPh_M.[13f] These differences have been attributed to the presence of a hydrogen bond between the C_9-keto group of BPh_L and a nearby glutamic acid residue.[8,11b,c] No equivalent interaction occurs in BPh_M. In the case of BPh_{film}, the breadth of the RR bands makes it difficult to clearly assess all of the spectral features, particularly in the 220−300-cm^{-1} region. However, a noteworthy feature of the spectrum of $BChl_{film}$ is that essentially all of the observed bands have analogs in the spectra of the BPh_L and BPh_M. This situation can be contrasted with that observed for the BChls in the solid aggregate versus protein environment (vide supra). The greater similarity between the spectra of the BPhs in the film versus protein environment is attributed to the fact that these cofactors cannot acquire axial ligands.

Vibrational Assignments. The vibrational assignments for the BChl and BPh pigments were determined in a stepwise and systematic fashion. The first step was to correlate the modes of the BChls or the BPhs based on isotope shift. The second step was to examine globally the spectra of all the pigments in order to identify modes which are common to all of the pigments. The third step was to compare the spectra of the pigments in the RCs versus the films. All of these steps were guided by the predictions of the semiempirical normal coordinate calculations. In this analysis, the assignment of the RR spectra of the BChls took precedence over that of the BPhs because many more bands of the former pigment exhibit isotope shifts. In addition, the BChls exhibit larger spectral differences in the protein versus film environments than do the BPhs.

In Table 3, vibrational assignments are presented only for the RR bands observed in the lower frequency portion (<250 cm^{-1}) of the spectral window which was investigated. Only these modes were assigned for the following reasons: (1) The strongly coupled modes of P, which are the focus of this study, are confined to this spectral region.[13d,14,18,23−26] (2) Approximately one-half of the modes observed for BChl below 250 cm^{-1} exhibit isotope shifts. In contrast, only one of the 10 or more modes observed in the 250−425-cm^{-1} region is sensitive to isotopic substitution. (3) In the 50−250-cm^{-1} region, the number of calculated modes exceeds the number observed by only three to four. In contrast, in the 250−425-cm^{-1} region, the number of calculated modes exceeds the number observed by 10 or more. The absence of isotope sensitivity in conjunction with the large number of calculated versus observed modes precludes a reliable assignment for most of the bands in the 250−425-cm^{-1} region. In the sections below, we first discuss the assignments of the isotope-sensitive vibrational modes. We then turn to the assignments for isotope-insensitive modes focusing only on the bands below 250 cm^{-1}.

1. ^{26}Mg-Sensitive Modes. The normal coordinate calculations predict that two modes of BChl below 250 cm^{-1} should exhibit appreciable ^{26}Mg isotope shifts (>0.5 cm^{-1}). These vibrations are the macrocycle doming mode, γMg_{dome}, calculated at 182 cm^{-1}, and the Mg(II)−histidine stretching mode, νMgN_{his}, calculated at 232 cm^{-1}. The pair of RR bands observed for both P_L and $BChl_{L,M}$ at ∼137 and ∼240 cm^{-1} are

assigned to these vibrations. [It should be noted that γMg_{dome} is predicted to involve predominantly metal ion motion, hence the absence of ^{15}N sensitivity.] The assignment of the protein−cofactor RR bands to γMg_{dome} and νMgN_{his} is qualitatively consistent with the absence of analogous bands for $BChl_{film}$. As was previously noted, the different types of axial ligation present in the film versus protein environment could significantly change the frequency and/or relative intensity of these vibrations and explain their absence from the RR spectrum of $BChl_{film}$. Recall also that the RR bands of $BChl_{L,M}$ attributed to γMg_{dome} and νMgN_{his} are extremely weak (Figure 8). Modes of similar intensity in the RR spectra of $BChl_{film}$ could easily be missed owing to the poorer quality of the isotope-difference data. The assignment of the remaining ^{26}Mg-sensitive mode, which is observed for P_L, $BChl_{L,M}$, and $BChl_{film}$ in the 179−203-cm^{-1} region, is less certain. As was noted above, the normal coordinate calculations do not predict the presence of a third mode with any appreciable ^{26}Mg isotope shift. However, the ^{26}Mg-sensitive vibrational feature in the 179−203-cm^{-1} region also exhibits an ^{15}N shift. The normal coordinate calculations predict that only one vibration in the spectral region below 250 cm^{-1} exhibits both a ^{26}Mg and ^{15}N isotope shift of any appreciable magnitude (the ^{26}Mg shifts for all other modes are <0.1 cm^{-1}). This vibration is calculated at 191 cm^{-1} which is in the center of the frequency range observed for the ^{26}Mg-/^{15}N-sensitive mode. The 191-cm^{-1} vibration is of highly mixed character containing metal doming and core deformations plus substituent group motions.

The somewhat unsatisfactory performance of the normal coordinate calculations in predicting the existence of the third ^{26}Mg-sensitive mode below 250 cm^{-1} is attributed to the fact that the optimized structure of the BChl macrocycle predicted by the QCFF/PI method exhibits less out-of-plane distortion than is observed for the BChl cofactors in the RC.[8] A larger out-of-plane distortion would promote more mixing between γMg_{dome}/νMgN_{his} and motions of the BChl core. The increased mixing would spread the ^{26}Mg shift among additional modes instead of localizing it primarily in γMg_{dome} and νMgN_{his}. [Note that the calculated ^{26}Mg shifts for both of these modes are larger than observed (Table 3).] In addition, the frequency of the former mode is calculated to be considerably higher than observed (182 versus 137 cm^{-1}). Mixing with other modes could bring the calculated frequency more in-line with the observed value. Regardless of these shortcomings, the frequencies and isotope-shift patterns (both ^{26}Mg and ^{15}N) predicted by the semiempirical normal coordinate calculations are remarkably consistent with those observed.

The normal coordinate calculations predict that a number of modes above 250 cm^{-1} should exhibit ^{26}Mg sensitivity. These modes are of highly mixed character containing contributions from a large number of internal coordinates. The ^{26}Mg sensitivity in all of these modes arises primarily from contributions of in-plane $Mg-N_{pyr}$ stretching character. Owing to the highly mixed nature of these vibrations, the relative amount of ^{26}Mg versus ^{15}N shift varies considerably among the modes. The ^{26}Mg-sensitive RR band observed for P_L, $BChl_{L,M}$, and $BChl_{film}$ at ∼364 cm^{-1} (which exhibits little or no ^{15}N shift) is assigned to one of these highly mixed vibrations.

2. ^{15}N-Sensitive Modes. The normal coordinate calculations predict that only two modes of BChl below 250 cm^{-1} should exhibit any appreciable ^{15}N isotope shifts (>1 cm^{-1}). These modes are calculated at 154 and 176 cm^{-1}, and both primarily involve out-of-plane deformations of the pyrrole rings. The pair of RR bands observed for P_L, $BChl_{L,M}$, and $BChl_{film}$ in the 137−154- and 181−203-cm^{-1} ranges is assigned to these modes. The calculations also predict that two modes of BPh below 250 cm^{-1} should exhibit appreciable ^{15}N isotope shifts. These modes are calculated at 127 and 171 cm^{-1} and again primarily involve out-of-plane deformations of the pyrrole rings. The single ^{15}N-sensitive RR band of the BPhs observed in the 138−150-cm^{-1} region is assigned to the deformation calculated at 127 cm^{-1} based on the closer frequency agreement and the fact that the vibrational eigenvector for this mode is qualitatively similar to that of the ^{15}N-sensitive mode of the BChls which occurs in a similar spectral region (137−154 cm^{-1}). The exact forms of the vibrational eigenvectors of these modes of BChl and BPh, although similar, are not sufficiently alike to be described as analogs. Hence, these modes are not correlated in Table 3.

3. Isotope-Insensitive Modes. The assignment of the remaining RR bands below 250 cm^{-1} is less certain owing to their insensitivity to isotopic substitution. However, certain general characteristics of these spectral features lend confidence to the assignments proposed in Table 3. In particular, approximately one-half of the isotope-insensitive RR bands are observed in the very low-frequency regime below 130 cm^{-1}. The normal coordinate calculations predict that vibrations in the 50−130-cm^{-1} region are exclusively due to deformations (primarily out-of-plane) of the peripheral substituent groups on the macrocycle. These types of modes also dominate this frequency regime for metalloporphyrins.[35,36] The calculations also predict that other deformations (primarily in-plane) of the substituent groups are interspersed with the macrocycle modes in the 130−250-cm^{-1} region. The fact that the isotope-insensitive RR bands of the BChls can be correlated with those of the BPhs in a one-to-one fashion (with the exception of a single BPh band) and that the frequencies of these bands of the different types of pigments are quite similar is a strong argument that these vibrations involve atomic motions well removed from the core of the macrocycle (cf. Figures 8 and 9).

The normal coordinate calculations predict that deformations of the substituent groups on all four pyrrole rings (rings I−IV) and the exocyclic ring (ring V) contribute to modes in the 50−425-cm^{-1} region. If deformations which primarily involve motions of the alkyl substituents on the saturated pyrrole rings (rings II and IV) are excluded from consideration, the number of calculated modes essentially matches the number of observed modes. As a first approximation, the exclusion of substituent vibrations on rings II and IV is reasonable given that these groups are on sections of the macrocycle that are outside the π-conjugation pathway. In making the assignments for the isotope-insensitive modes shown in Table 3, we have matched the observed and calculated modes such that the frequency ordering of the calculated modes remains sequential. In the absence of additional information, there is no basis for assigning modes out of sequence.

With the above considerations, the RR bands of the BChls and BPhs observed in the 56−72-, 87−96-, and 118−131-cm^{-1} ranges are all assigned to vibrations which primarily involve the acetyl and methyl substituents on ring I (Figure 2). Specifically, these bands are assigned to the out-of-plane deformation of the C_2-acetyl methyl group, $\gamma C_{acetyl}CH_3$, calculated at 63 cm^{-1} (BChl) and 74 cm^{-1} (BPh), the out-of-plane deformation of the ring I methyl group, γC_bCH_3(I), calculated at ∼84 cm^{-1} (BChl and BPh), and the in-plane deformation of the C_2-acetyl group, δC_2C_{acetyl}, calculated at 131 cm^{-1} (BChl) and 121 cm^{-1} (BPh). The RR spectra so provide some

(35) Li, X.-Y.; Czernuszewicz, R. S.; Kincaid, J. R. *J. Am. Chem. Soc.* **1989**, *111*, 7312−7323.

(36) (a) Hu, S.; Morris, I. K.; Singh, J. P.; Smith, K. M.; Spiro, T. G. *J. Am. Chem. Soc.* **1993**, *115*, 12446−12458. (b) Hu, S.; Smith, K. M.; Spiro, T. G. *J. Am. Chem. Soc.*, submitted.

additional experimental evidence in support of these assignments. In particular, these modes of P_L, particularly those which involve vibrations of the C_2-acetyl group (72 and 130 cm^{-1}), are uniformly at higher frequencies than those of $BChl_{L,M}$ (56 and 118 cm^{-1}). Such differences might be anticipated owing to the fact that the C_2-acetyl group of P_L is hydrogen bonded to a histidine residue of the protein, whereas the C_2-acetyl groups of $BChl_{L,M}$ are free.[8d,e,9−11b−d] Axial ligation involving the C_2-acetyl groups in $BChl_{film}$ could also explain the different RR scattering characteristics observed for the acetyl group modes of $BChl_{film}$ versus P_L or $BChl_{L,M}$. [Recall that these modes of the film are absent or much weaker than for the protein (Figure 8).] The normal coordinate calculations also suggest that the ∼35-cm^{-1} RR band of P_L reported by Mathies, Boxer, and coworkers[14] can be attributed to an acetyl group vibration. [This RR band is not observed in our studies because experimental limitations preclude access to this frequency regime.] Only three modes are calculated in the 30−50-cm^{-1} region, and all contain substantial C_2-acetyl group motion,. The ∼35-cm^{-1} band of P_L is assigned to the out-of-plane deformation of this group, γC_2C_{acetyl}, because the calculated frequency of this mode (30 cm^{-1}) is closest among the three to the observed value.

The remaining isotope-insensitive RR bands of the BChls and BPhs observed in the 144−166-, 179−187-, and 208−240-cm^{-1} ranges are assigned to in-plane deformations of substituent groups which are calculated at 160, 198, and 221 cm^{-1} for BChl and at 153, 195, and 216 cm^{-1} for BPh. All of these modes are of highly mixed character, and only the largest contributors to the vibrational eigenvectors are listed in Table 3. It should also be noted that motions of the ring II and IV substituent groups are predicted to participate in certain vibrations, particularly the modes in the 179−187-cm^{-1} region. The assignment of RR bands to modes involving these substituents is necessitated by the absence of any other calculated modes in this frequency regime. Finally, the lone remaining isotope-insensitive RR band, a BPh mode observed in the 137−146-cm^{-1} region, is assigned to an out-of-plane deformation of the macrocycle, specifically the γring III (swivel), calculated at 138 cm^{-1}. The analogous vibration of BChl is neither observed nor calculated in this frequency regime. The swiveling motion of the pyrrole ring is not sensitive to ^{15}N substitution because the swivel axis contains the nitrogen atom.[35]

Strong Vibronic Coupling in P and Implications for Functional Activity. The vibrational assignments for the low-frequency modes of the BChls and BPhs provide a benchmark for elucidating the nature of the vibrations of P which are strongly coupled to the photophysically important, lowest energy electronic transition. Previous spectroscopic studies of P have shown that the strongly coupled modes are primarily clustered in the region below 150 cm^{-1}.[13d,14,18d,24−28] Modes near 35 and 135 cm^{-1} have received particular attention. The 135-cm^{-1} vibration has been characterized as a "marker mode" of the primary electron donor.[25] It has been suggested that this mode could correspond to an intradimer vibration arising from motions along coordinates corresponding to the additional degrees of freedom of the supermolecule.[25,27,37,38] In contrast, we have argued that all of the RR bands observed for P above 50 cm^{-1} are due to vibrations intrinsic to a BChl molecule.[13d,18d] This argument was based primarily on the fact that a one-to-one correspondence can be found for the RR bands of P and the accessory BChls in this frequency regime. In addition, a frequency of 135 cm^{-1} is much higher than would be expected for an intradimer mode. The isotopic substitution experiments reported herein provide additional compelling support to our proposal that the "marker mode" of P is due to intramolecular vibrations of the BChl molecule. In particular, the isotope data indicate that the feature near 135 cm^{-1} is actually a cluster of three near-coincident vibrations, two of which exhibit significant isotope shifts. Modes with similar isotope shifts are observed for $BChl_{L,M}$. In addition, the magnitudes of the isotope shifts are much larger than would be expected for a true intradimer vibration. The remaining isotope-insensitive mode in the cluster of three can also be reasonably assigned as an intramolecular vibration of a BChl molecule. We cannot rule out the possibility that the 35-cm^{-1} band of P is due to an intradimer mode or to a vibration of the protein matrix, as has been suggested for certain strongly coupled, very low-frequency modes.[27] However, the normal coordinate calculations also provide a reasonable assignment for this mode in terms of an intramolecular vibration of a BChl molecule. The fact that this vibration appears to be localized on ring I provides additional support for an intramolecular characterization (vide infra).

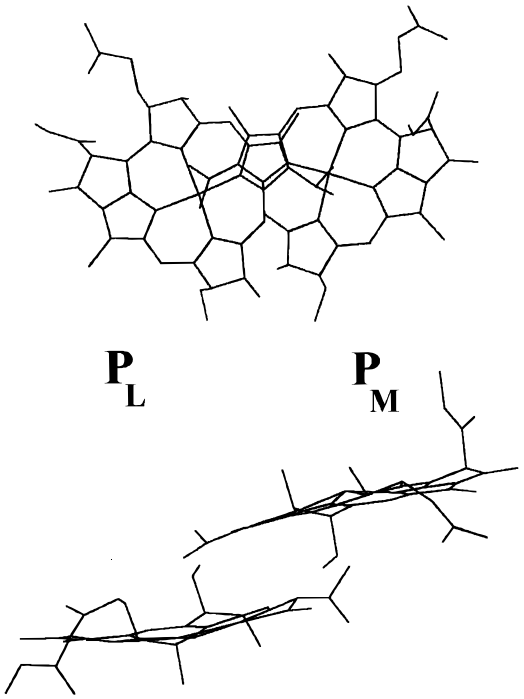

Figure 10. Two views of P in RCs from *Rb. sphaeroides*. The bottom view is along the approximate C_2 symmetry axis of the dimer; the top view is approximately orthogonal to this axis.[8d]

The assignments for the low-frequency modes of P_L in conjunction with the structure of the dimer provide an explanation as to why certain intramolecular vibrations of this cofactor are strongly coupled to the P* transition. An enlarged view of P in *Rb. sphaeroides* shown from two different perspectives is shown in Figure 10.[8d] The bottom view is along the approximate C_2 symmetry axis of the dimer; the top view is approximately orthogonal to this axis. These views illustrate the overlap between P_L and P_M, which primarily involves ring I, and the concomitant positioning of the C_2-acetyl substituents of each cofactor in immediate proximity to the core of the adjacent macrocycle. This geometrical arrangement of P_L and P_M suggests that deformations localized on ring I and the macrocycle core could be particularly effective at modulating the electronic structure of the dimer. Indeed, the vibrational assignments indicate that these types of motions are the prime contributors to the vibrational eigenvectors of all the modes below 150 cm^{-1}. In particular, the cluster of three intense RR bands of P_L which contribute to the 135-cm^{-1} "marker mode"

(37) Warshel, A. *Proc. Natl. Acad. Sci. U.S.A* **1980**, *77*, 3105−3109.
(38) Lathrop, E.; Friesner, R. A. *J. Phys. Chem.* **1994**, *98*, 3056−3066.

all involve motions localized on the C_2-acetyl group (δC_2C_{acetyl}, 130 cm^{-1}) or the macrocycle core (γMg_{dome}, 137 cm^{-1}; γrings I−IV (tilt, translation), 143 cm^{-1}). Deformations of the C_2-acetyl group are ideal candidates for modulating the electronic structure of the dimer because this group is conjugated into the π-electron system of the macrocycle.[39] Motions of the highly polarizable carbonyl group on one cofactor could also modulate the electronic structure of the dimer via a through-space mechanism. The γC_2C_{acetyl} vibration, assigned to the strongly coupled, 35-cm^{-1} mode, should be particularly effective at modulating the electronic structure via the latter mechanism because this motion moves the carbonyl group approximately orthogonal to the plane of the macrocycle. Any of the motions of the acetyl group could influence the relative energies of the molecular orbitals. In addition, if the two halves of the dimer are influenced differently, the inequivalence of the two rings will be modulated. This in turn could strongly influence the charge-transfer character known to be present in the P* state.[4,5,23b,38,40,41] This propensity makes the assignment of the 35-cm^{-1} mode to γC_2C_{acetyl} even more attractive.

The question remains as to whether the strong coupling exhibited by the low-frequency modes of the ring I substituents and the macrocycle core plays any role in mediating the electron-transfer process in RCs or is just a consequence of the geometrical arrangement of the two cofactors which has no functional significance. In this regard, a number of theoretical studies have predicted that the C_2-acetyl groups mediate the electronic properties of P and could thereby influence the electron-transfer process.[42−45] Recent electrostatic calculations on RCs have also predicted that the orientation of the C_2-acetyl groups has a significant influence on the redox potential of P.[45] Accordingly, deformations of this group could certainly modulate the electron density in the supermolecule and potentially mediate the initial charge separation event. From a functional standpoint, it is also appealing that multiple BChl vibrations are strongly coupled to the P* electronic transition. Presumably, the participation of multiple (rather than a single) mediating modes could provide for more robust control of the electronic properties which control charge separation.

Conclusions

The isotope-assisted vibrational assignments proposed for the BChls and BPhs provide a self-consistent picture of the characteristics of the very low-frequency (<250-cm^{-1}), RR active modes of these pigments. Together, the assignments for all of the pigments in both the RCs and films permit the development of a reasonable and consistent picture of the nature of the strongly coupled, low-frequency modes of P. The picture which emerges, namely, that the strongly coupled modes involve motions localized on pyrrole ring I and the macrocycle core, is logically consistent with the structure of the dimer. The unique interplay between the structural, electronic, and vibronic characteristics of the primary electron donor suggests that the strong coupling of certain vibrations is an intrinsic consequence of the geometrical arrangement of the cofactors and may have important functional ramifications.

Acknowledgment. This work was supported by Grants GM39781 (D.F.B) (protein studies), GM36243 (D.F.B) (film studies), and GM30353 (H.A.F.) from the National Institute of General Medical Sciences, the Cooperative State Research Service, USDA, under Agreement No. 92-37306-7690 (H.A.F.), and the Human Frontier of Science Program (H.A.F.). K.C. thanks M. Sykora for providing some of the software used for fitting the difference spectra.

JA963281C

(39) Gudowska-Nowak, E.; Newton, M. D.; Fajer, J. *J. Phys. Chem.* **1990**, *94*, 5795−5801.

(40) (a) Parson, W. W.; Warshel, A. *J. Am. Chem. Soc.* **1987**, *109*, 6152−6163. (b) Thompson, M. A.; Zerner, M. C.; Fajer, J. *J. Phys. Chem.* **1991**, *95*, 5693−5700. (c) Scheer, P. O. J.; Fischer, S. In *Chlorophylls*; Scheer, H., Ed.; CRC Press: Boca Raton, FL, 1991; pp 1079−1093. (d) Scheer, P. O. J.; Fischer, S. In ref 6, pp 193−207.

(41) (a) Lösche, M.; Feher, G.; Okamura, M. *Proc. Natl. Acad. Sci. U.S.A* **1987**, *84*, 7537−7541. (b) Lockhart, D. J.; Boxer, S. G. *Proc. Natl. Acad. Sci. U.S.A* **1988**, *85*, 107−111.

(42) (a) Scheer, P. O. J.; Fischer, S. *Chem. Phys.* **1987**, *115*, 151−158. (b) Scheer, P. O. J.; Fischer, S. *Chem. Phys*. **1989**, 131, 115−129.

(43) Parson, W. W.; Nabedryk, E.; Breton, J. In ref 6, pp 79−88.

(44) Barkigia, K.; Fajer, J. In ref 7, pp 513−540 and references therein.

(45) (a) Muegge, I.; Apostolakis, J.; Ermler, U.; Fritzsch, G.; Lubitz, W.; Knapp, E. W. *Biochemistry* **1996**, *35*, 8359−8370. (b) Apostolakis, J.; Muegge, I.; Ermler, U.; Fritzsch, G.; Knapp, E. W. *J. Am. Chem. Soc.* **1996**, *118*, 3743−3752.